3

Dendrites and synapses

Neurons have intricate morphologies: the central part of the cell is the soma, which contains the genetic information and a large fraction of the molecular machinery. At the soma originate long wire-like extensions which come in two different flavors. First, the dendrites form a multitude of smaller or larger branches on which synapses are located. The synapses are the contact points where information from other neurons (i.e., "presynaptic" cells) arrives. Second, also originating at the soma, is the axon, which the neuron uses to send action potentials to its target neurons. Traditionally, the transition region between soma and axon is thought to be the crucial region where the decision is taken whether a spike is sent out or not.

The Hodgkin–Huxley model, at least in the form presented in the previous chapter, disregards this spatial structure and reduces the neuron to a point-like spike generator – despite the fact that the precise spatial layout of a neuron could potentially be important for signal processing in the brain. In this chapter we will discuss how some of the spatial aspects can be taken into account by neuron models. In particular we focus on the properties of the synaptic contact points between neurons and on the electrical function of dendrites.

3.1 Synapses

In the previous chapter, we have encountered two classes of ion channels, namely *voltage*-activated and *calcium*-activated ion channels. The third type of ion channel we have to deal with are the *transmitter*-activated ion channels involved in synaptic transmission (see Fig. 3.1) and generally activated from outside the cell. Activation of a presynaptic neuron results in a release of neurotransmitters into the synaptic cleft. The transmitter molecules diffuse to the other side of the cleft and activate receptors that are located in the postsynaptic membrane. So-called *ionotropic receptors* have a direct influence on the state of an associated ion channel. *Metabotropic receptors* control the state of an ion channel by means of a biochemical cascade of G proteins and second-messengers. In both cases, the activation of the receptor results in the opening of certain ion channels and, thus, in an excitatory or inhibitory postsynaptic transmembrane current (EPSC or IPSC).

Instead of developing a mathematical model of the transmitter concentration in the synaptic cleft, we keep things simple and describe transmitter-activated ion channels as

https://doi.org/10.1017/CBO9781107447615.004 Published online by Cambridge University Press

an explicitly time-dependent conductivity $g_{\rm syn}(t)$ that will open whenever a presynaptic spike arrives. The current that passes through a synaptic channel depends, as before, on the difference between its reversal potential $E_{\rm syn}$ and the actual value of the membrane potential,

$$I_{\rm syn}(t) = g_{\rm syn}(t)\,(u(t) - E_{\rm syn})\,. \tag{3.1}$$

The parameter $E_{\rm syn}$ and the function $g_{\rm syn}(t)$ can be used to describe different types of synapses. For inhibitory synapses $E_{\rm syn}$ is usually set to $-75\,{\rm mV}$, whereas for excitatory synapses $E_{\rm syn} \approx 0$.

Typically, a superposition of exponentials is used for $g_{\rm syn}(t)$. A simple choice for the time course of the synaptic conductance in Eq. (3.1) is an exponential decay

$$g_{\rm syn}(t) = \sum_f \bar{g}_{\rm syn}\, e^{-(t-t^f)/\tau}\,\Theta(t-t^f)\,, \tag{3.2}$$

with a time constant of, e.g., $\tau = 5\,{\rm ms}$ and an amplitude of $\bar{g}_{\rm syn} = 40\,{\rm pS}$. Here, t^f denotes the arrival time of a presynaptic action potential and $\Theta(x)$ is the Heaviside step function.

For some synapse types, a single exponential decay is not sufficient. Rather, the postsynaptic current is made up of two different components, a fast one with a decay time constant of a few milliseconds, and a second one that is often ten times slower. If we also take into account the smooth rise of the synaptic response, the postsynaptic conductance is of the form

$$g_{\rm syn}(t) = \sum_f \bar{g}_{\rm syn}\,[1 - e^{-(t-t^f)/\tau_{\rm rise}}]\,\left[a\,e^{-(t-t^f)/\tau_{\rm fast}} + (1-a)\,e^{-(t-t^f)/\tau_{\rm slow}}\right]\Theta(t-t^f)\,, \tag{3.3}$$

where a is the relative weight of the fast component. The time constant $\tau_{\rm rise}$ characterizes the rise time of the synaptic conductance.

Example: A more detailed synapse model

Instead of considering a synapse with a fixed time course $g_{\rm syn}(t)$, we can also make a model which has the flavor of a Hodgkin–Huxley channel. We describe the synaptic conductance $g_{\rm syn}(t) = g_{\rm max}\,R(t)$, by its maximal conductance $g_{\rm max}$ and a gating variable R, where $R(t)$ is the fraction of open synaptic channels. Channels open when neurotransmitter N binds to the synapse

$$\frac{{\rm d}R}{{\rm d}t} = \alpha\,N\,(1-R) - \beta\,R, \tag{3.4}$$

where α is the binding constant, β the unbinding constant and $(1-R)$ the fraction of closed channels where binding of neurotransmitter can occur. Neurotransmitter N is released with each presynaptic spike so that the total amount of neurotransmitter at synapse j is

$$N(t) = \int_0^\infty \gamma(s)\,S_j(t-s)\,{\rm d}s, \tag{3.5}$$

https://doi.org/10.1017/CBO9781107447615.004 Published online by Cambridge University Press

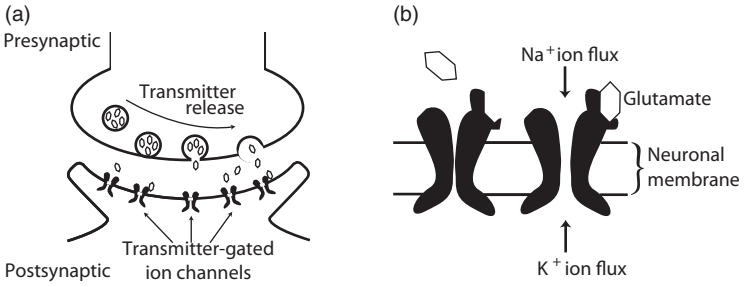

Fig. 3.1 (a) Schema of synaptic transmission. Upon arrival of a presynaptic spike, neurotransmitter spills into the synaptic cleft and is captured by postsynaptic receptors. (b) Schema of a postsynaptic AMPA[1] receptor of an excitatory synapse. When glutamate is bound to the receptor, sodium and potassium ions can flow through the membrane.

where $S_j = \sum_f \delta(t - t_j^f)$ is the presynaptic spike train (a sequence of δ-functions, see Chapter 1) and $\gamma(s)$ is the time course of the neurotransmitter density as measured at the site of the postsynaptic receptor. More advanced synaptic signaling schemes can be designed along the same line of argument (Destexhe *et al*., 1994b).

3.1.1 Inhibitory synapses

The effect of fast inhibitory neurons in the central nervous system of higher vertebrates is almost exclusively conveyed by a neurotransmitter called γ-aminobutyric acid, or GABA for short. A characteristic feature of inhibitory synapses is that the reversal potential E_{syn} is in the range of -70 to -75 mV. Thus, if the neuronal membrane potential is above the reversal potential, presynaptic spike arrival leads to a hyperpolarization of the neuron, making action potential generation less likely. However, the same presynaptic spike would lead to a depolarization of the membrane if the neuron has its membrane potential at -80 mV or below.

There are many different types of inhibitory interneurons (Markram *et al*., 2004; Klausberger and Somogyi, 2008). Biologists distinguish between two major types of inhibitory synapse, called GABA_A and GABA_B. Both synapse types use GABA as the neurotransmitter. GABA_A channels are ionotropic and open exclusively for chloride ions, whereas GABA_B synapses have metabotropic receptors that trigger a comparatively slow signaling chain ultimately leading to the opening of K^+ channels. Consequently the value of the synaptic reversal potential E_{syn} depends for GABA_A synapses on the concentration of chloride ions inside and outside the cell, while that of GABA_B synapses depends on the potassium concentrations.

[1] AMPA is short for α-amino-3-hydroxy-5-methyl-4-isoxalone propionic acid.

https://doi.org/10.1017/CBO9781107447615.004 Published online by Cambridge University Press

Example: $GABA_A$ synapse model

$GABA_A$ synapses have a fast time course that can be approximated by a single term in Eq. (3.3) with $a = 1$, $\tau_{rise} \approx 1$ ms, and a time constant $\tau_{fast} \approx 6$ ms (Destexhe and Pare (1999); Fig. 3.2), which has also been deemed 3 times larger. More complex models are sometimes used (Destexhe *et al*., 1994b).

Example: $GABA_B$ synapse model

This is a slow inhibitory synapse working via a second-messenger chain. Common models use Eq. (3.3) with a rise time of about 25–50 ms, a fast decay time in the range of 100–300 ms and a slow decay time of 500–1000 ms. The fast component accounts for about 80% of the amplitude of conductance ($a = 0.8$) (Destexhe *et al*., 1994b; McCormick *et al*., 1993), illustrated in Fig. 3.2.

3.1.2 Excitatory synapses

Most excitatory synapses in the vertebrate central nervous system rely on glutamate as their neurotransmitter. The postsynaptic receptors, however, can have very different pharmacological properties and different types of glutamate receptor units can be present in a single synapse. These receptors are classified using artificial drugs such as NMDA or AMPA that act as selective agonists. NMDA (N-methyl-D-aspartate) binds to channels with NMDA receptors, but not to other glutamate receptors. The most prominent among those glutamate receptors that do not respond to NMDA are the AMPA-receptors. AMPA is an artificial glutamate. Channels with AMPA-sensitive receptors are called "AMPA channels" because these channels react to AMPA, whereas channels with NMDA-sensitive receptors do not open upon application of AMPA. However, both NMDA and AMPA channels react to the natural form of glutamate that the nervous system uses as neurotransmitter.

AMPA receptors consist of four subunits, each with a glutamate binding site. Most AMPA receptors contain the subunit called GluR2. If an AMPA-receptor channel containing GluR2 is open, sodium and potassium ions can pass, but calcium ions cannot. Synaptic channels with AMPA-receptors are characterized by a fast response to presynaptic spikes and a quickly decaying postsynaptic current.

NMDA-receptor controlled channels are significantly slower and have additional interesting properties that are due to a voltage-dependent block by magnesium ions (Hille, 1992). In addition to sodium and potassium ions, also calcium ions can pass through open NMDA-channels.

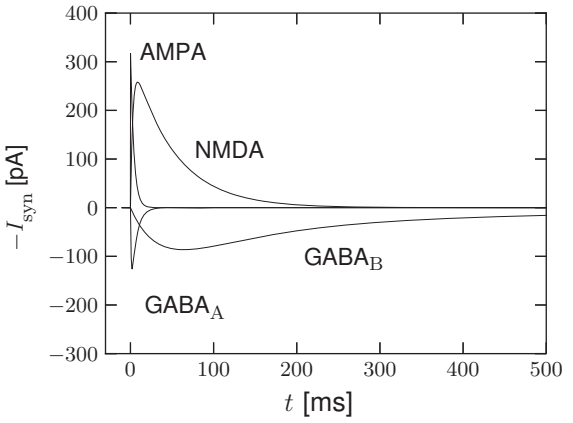

Fig. 3.2 Dynamics of postsynaptic current (3.1) after a single presynaptic spike at $t = 0$. $GABA_A$, $GABA_B$, AMPA, and NMDA without magnesium block are shown for a postsynaptic neuron at rest ($u = -65$mV).

Example: Conductance of glutamate channels with AMPA-receptors

The time course of the postsynaptic conductivity caused by an activation of AMPA-receptors at time $t = t^f$ is sometimes described by Eq. (3.2) with a decay time of about 2–5 ms (Gabbiani *et al*., 1994; Destexhe *et al*., 1994b).

Example: Conductance of glutamate channels with NMDA-receptors

NMDA-receptor controlled channels exhibit a rich repertoire of dynamic behavior because their state is controlled not only by the presence or absence of glutamate, but also by the membrane potential. At resting potential the NMDA channel is blocked by a common extracellular ion, Mg^{2+}, even if glutamate is present (Hille, 1992). Even in the presence of glutamate, the channel remains closed at the resting potential. If the membrane is depolarized beyond -50 mV, the Mg^{2+}-block is removed, the channel opens when glutamate binds to the receptor and, thereafter, stays open for 10–100 ms. A simple model of the voltage dependence of NMDA-receptor controlled channels is

$$g_{\rm NMDA}(t) = \bar{g}_{\rm NMDA} \cdot \left[1 - {\rm e}^{-(t-t^f)/\tau_{\rm rise}}\right] {\rm e}^{-(t-t^f)/\tau_{\rm decay}}\, g_\infty(u, [{\rm Mg}^{2+}]_{\rm o})\, \Theta(t-t^f)\,,$$
$$\text{with } g_\infty(u, [{\rm Mg}^{2+}]_{\rm o}) = \left(1 + \beta\, {\rm e}^{\alpha u}\, [{\rm Mg}^{2+}]_{\rm o}\right)^{-1}\,, \quad (3.6)$$

with $\tau_{\rm rise}$ in the range of 3 ms to 15 ms, $\tau_{\rm decay}$ in the range of 40 ms to 100 ms, $\bar{g}_{\rm NMDA} = 1.5$ nS, $\alpha = -0.062\,{\rm mV}^{-1}$, $\beta = 1/(3.57{\rm mM})$, and an extracellular magnesium concentration $[{\rm Mg}^{2+}]_{\rm o} = 1.2$ mM (McCormick *et al*., 1993; Gabbiani *et al*., 1994).

What is the potential functional role of NMDA receptors? First, their comparatively long time constant keeps a trace of presynaptic events and acts as a low-pass filter. Second, even though NMDA-receptor controlled ion channels are permeable to sodium and potassium ions, their permeability to Ca^{2+} is five or ten times larger. Calcium ions are known to play an important role in intracellular signalling and are probably involved in

https://doi.org/10.1017/CBO9781107447615.004 Published online by Cambridge University Press

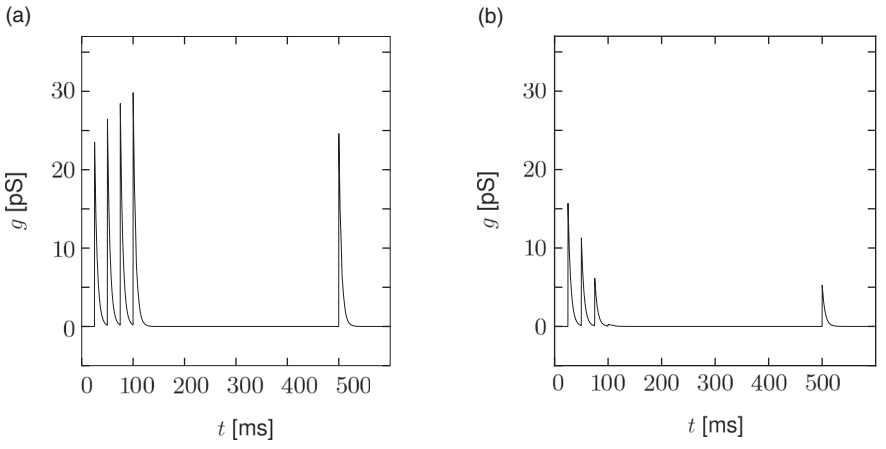

Fig. 3.3 Short-term plasticity. A synapse is activated by four presynaptic spikes and a fifth spike 400 ms later. (a) At a facilitating synapse, the effect of the second and third spike is larger than that of the first spike. The effect of a spike after a pause of 400 ms is approximately that of the first spike (time constant $\tau_P = 200$ ms). (b) At a depressing synapse, successive spikes in a periodic spike train have less and less effect: 400 ms later, the synapse has partially recovered, but is still significantly depressed ($\tau_P = 500$ ms).

long-term modifications of synaptic efficacy. Calcium influx through NMDA-controlled ion channels can occur if presynaptic spike arrival (leading to glutamate release from presynaptic sites) coincides with a depolarization of the postsynaptic membrane (leading to removal of the Mg^{2+}-block). Hence, NMDA-receptors operate as molecular coincidence detectors between pre- and postsynaptic events.

3.1.3 Rapid synaptic dynamics

Parameters of a synaptic contact point are not fixed, but can change as a function of the stimulation history. Some of these changes are long-lasting and are thought to represent the neuronal correlate of learning and memory formation. The description of these learning-related changes will be covered in Chapter 19. Here we concentrate on dynamic changes of the synapse that do not persist but decay back to their normal values within hundreds of milliseconds or a few seconds. These changes are called short-term synaptic plasticity.

Short-term synaptic plasticity can be measured if a presynaptic neuron is stimulated so as to generate a sequence of spikes. Synaptic facilitation means that the apparent amplitude of a postsynaptic current in response to the second spike is larger than that to the first spike. Synaptic depression is the opposite effect (Fig. 3.3).

As a simple model of synaptic facilitation and depression (Dayan and Abbott, 2001), we assume that the maximal synaptic conductance $\bar{g}_{\rm syn}$ in Eq. (3.2) or (3.3) depends on the fraction $P_{\rm rel}$ of presynaptic sites releasing neurotransmitter. Facilitation and depression can both be modeled as presynaptic processes that modify $P_{\rm rel}$. With each presynaptic spike, the number of available presynaptic release sites changes. Between spikes the value of $P_{\rm rel}$

https://doi.org/10.1017/CBO9781107447615.004 Published online by Cambridge University Press

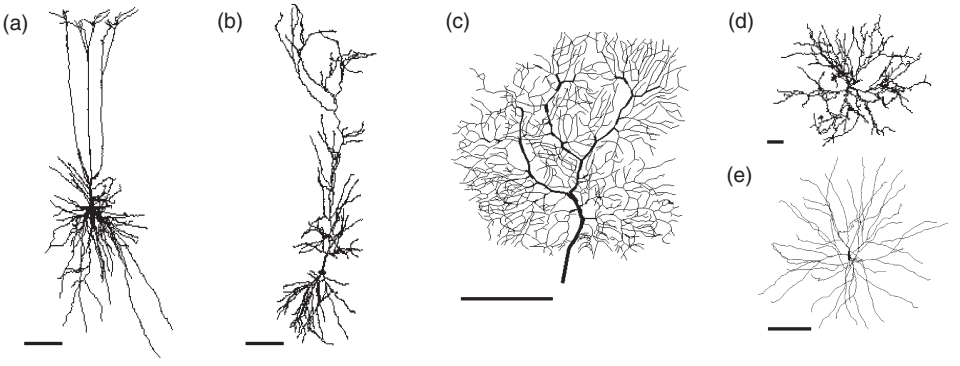

Fig. 3.4 Reconstructed morphology of various types of neurons. (a) Pyramidal neuron from a deep cortical layer (Contreras *et al*., 1997). (b) Pyramidal neuron from the CA1 of the hippocampus (Golding *et al*., 2005). (c) Purkinje cell from the cerebellum (Rapp *et al*., 1994). (d) Motoneuron from the spinal cord (Cullheim *et al*., 1987). (e) Stellate neuron from the neocortex (Mainen and Sejnowski, 1996). Reconstructed morphologies can be downloaded from http://NeuroMorpho.Org. Scale bars represent 100 μm.

returns exponentially to its resting value P_0. Thus,

$$\frac{\mathrm{d}P_{\mathrm{rel}}}{\mathrm{d}t} = -\frac{P_{\mathrm{rel}} - P_0}{\tau_P} + f_{\mathrm{F}}(1 - P_{\mathrm{rel}}) \sum_f \delta(t - t^f) \tag{3.7}$$

where τ_P is a time constant, f_{F} controls the degree of facilitation, and t^f denotes the times of presynaptic spike arrivals.

The model of a depressing synapse is completely analogous. The amount of neurotransmitter available for release develops according to the differential equation

$$\frac{\mathrm{d}P_{\mathrm{rel}}}{\mathrm{d}t} = -\frac{P_{\mathrm{rel}} - P_0}{\tau_P} - f_{\mathrm{D}} P_{\mathrm{rel}} \sum_f \delta(t - t^f) \tag{3.8}$$

where τ_P is a time constant and the parameter f_{D} with $0 < f_{\mathrm{D}} < 1$ controls the amount of depression per spike.

The total effect of presynaptic spikes depends on the available neurotransmitter as well as the value g_0 of postsynaptic conductance if all synaptic ion channels are open, so that, for depressing or facilitating synapses, we can use Eq. (3.2) with a value $\bar{g}_{\mathrm{syn}} = P_{\mathrm{rel}}\, g_0$. This procedure has been used to generate Fig. 3.3.

3.2 Spatial structure: the dendritic tree

Neurons in the cortex and other areas of the brain often exhibit highly developed dendritic trees that may extend over several hundred microns (Fig. 3.4). Synaptic input to a neuron is mostly located on its dendritic tree. Disregarding NMDA- or calcium-based electrogenic "spikes," action potentials are generated at the soma near the axon hillock. Up to now we

https://doi.org/10.1017/CBO9781107447615.004 Published online by Cambridge University Press

have discussed point neurons only, i.e., neurons without any spatial structure. What are the consequences of the spatial separation of input and output?

The electrical properties of point neurons have been described as a capacitor that is charged by synaptic currents and other *transversal* ion currents across the membrane. A non-uniform distribution of the membrane potential on the dendritic tree and the soma induces additional *longitudinal* current along the dendrite. We are now going to derive the cable equation that describes the membrane potential along a dendrite as a function of time *and* space. In Section 3.4 we shall see how geometric and electrophysiological properties can be integrated in a comprehensive biophysical model.

3.2.1 Derivation of the cable equation

Consider a piece of dendrite decomposed into short cylindric segments of length $\mathrm{d}x$ each. The schematic drawing in Fig. 3.5 shows the corresponding circuit diagram. Using Kirchhoff's laws we find equations that relate the voltage $u(x)$ across the membrane at location x with longitudinal and transversal currents. First, a longitudinal current $i(x)$ passing through the dendrite causes a voltage drop across the longitudinal resistor R_L according to Ohm's law,

$$u(t,x+\mathrm{d}x) - u(t,x) = R_\mathrm{L}\, i(t,x)\,, \tag{3.9}$$

where $u(t,x+\mathrm{d}x)$ is the membrane potential at the neighboring point $x+\mathrm{d}x$. Second, the transversal current that passes through the RC-circuit is given by $C\,\partial u(t,x)/\partial t + \sum_\mathrm{ion} I_\mathrm{ion}$ where the sum runs over all ion channel types present in the dendrite. Kirchhoff's law regarding the conservation of current at each node leads to

$$i(t,x+\mathrm{d}x) - i(t,x) = C\,\frac{\partial}{\partial t}\,u(t,x) + \sum_\mathrm{ion} I_\mathrm{ion} - I_\mathrm{ext}(t,x)\,. \tag{3.10}$$

The values of the longitudinal resistance R_L, the capacity C, the ionic currents as well as the externally applied current can be expressed in terms of specific quantities per unit length r_L, c, i_ion and i_ext, respectively, namely

$$R_\mathrm{L} = r_\mathrm{L}\,\mathrm{d}x\,, \quad C = c\,\mathrm{d}x\,, \quad I_\mathrm{ext}(t,x) = i_\mathrm{ext}(t,x)\,\mathrm{d}x\,, \quad I_\mathrm{ion}(t,x) = i_\mathrm{ion}(t,x)\,\mathrm{d}x\,. \tag{3.11}$$

These scaling relations express the fact that the longitudinal resistance and the capacity increases with the length of the cylinder. Similarly, the total amount of transversal current increases with the length $\mathrm{d}x$ simply because the surface through which the current can pass is increasing. Substituting these expressions in Eqs. (3.9) and (3.10), dividing by $\mathrm{d}x$, and taking the limit $\mathrm{d}x \to 0$ leads to

$$\frac{\partial}{\partial x}\,u(t,x) = r_\mathrm{L}\, i(t,x) \tag{3.12a}$$

$$\frac{\partial}{\partial x}\,i(t,x) = c\,\frac{\partial}{\partial t}\,u(t,x) + \sum_\mathrm{ion} i_\mathrm{ion}(t,x) - i_\mathrm{ext}(t,x)\,. \tag{3.12b}$$

https://doi.org/10.1017/CBO9781107447615.004 Published online by Cambridge University Press

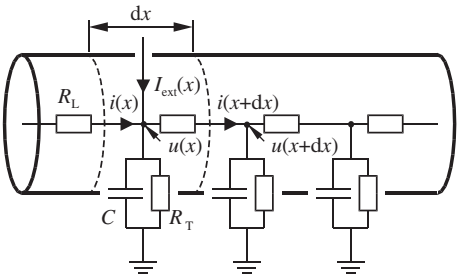

Fig. 3.5 Part of a dendrite and the corresponding circuit diagram. Longitudinal and transversal resistors are denoted by R_L and R_T, respectively. The electrical capacity of each small piece of dendrite is symbolized by capacitors C.

Taking the derivative of equation (3.12a) with respect to x and substituting the result into (3.12b) yields

$$\frac{\partial^2}{\partial x^2} u(t,x) = c\, r_L \frac{\partial}{\partial t} u(t,x) + r_L \sum_{\text{ion}} i_{\text{ion}}(t,x) - r_L\, i_{\text{ext}}(t,x). \tag{3.13}$$

Equation (3.13) is called the general cable equation.

Example: Cable equation for passive dendrite

The ionic currents $\sum_{\text{ion}} i_{\text{ion}}(t,x)$ in Eq. (3.13) can in principle comprise many different types of ion channel, as discussed in Section 2.3. For simplicity, the dendrite is sometimes considered as passive. This means that the current density follows Ohm's law $\sum_{\text{ion}} i_{\text{ion}}(t,x) = g_l(u - E_l)$ where $g_l = 1/r_T$ is the leak conductance per unit length and E_l is the leak reversal potential.

We introduce the characteristic length scale $\lambda^2 = r_T/r_L$ ("electrotonic length scale") and the membrane time constant $\tau = r_T c$. If we multiply Eq. (3.13) by λ^2 we get

$$\lambda^2 \frac{\partial^2}{\partial x^2} u(t,x) = \tau \frac{\partial}{\partial t} u(t,x) + [u(t,x) - E_l] - r_T\, i_{\text{ext}}(t,x). \tag{3.14}$$

After a transformation to unit-free coordinates,

$$x \to \hat{x} = x/\lambda\,, \quad t \to \hat{t} = t/\tau\,, \tag{3.15}$$

and a rescaling of the current and voltage variables,

$$i \to \hat{i} = \sqrt{r_T\, r_L}\, i\,, \quad i_{\text{ext}} \to \hat{i}_{\text{ext}} = r_T\, i_{\text{ext}}\,, \quad u \to \hat{u} = u - E_l, \tag{3.16}$$

we obtain the cable equation (where we have dropped the hats)

$$\frac{\partial}{\partial t} u(t,x) = \frac{\partial^2}{\partial x^2} u(t,x) - u(t,x) + i_{\text{ext}}(t,x), \tag{3.17}$$

in an elegant unit-free form.

https://doi.org/10.1017/CBO9781107447615.004 Published online by Cambridge University Press

The cable equation can be easily interpreted. The change in time of the voltage at location x is determined by three different contributions. The first term on the right-hand side of Eq. (3.17) is a diffusion term that is positive if the voltage is a convex function of x. The voltage at x thus tends to increase, if the values of u are higher in a neighborhood of x than at x itself. The second term on the right-hand side of Eq. (3.17) is a simple decay term that causes the voltage to decay exponentially towards zero. The third term, finally, is a source term that acts as an inhomogeneity in the otherwise autonomous differential equation. This source can be due to an externally applied current or to synaptic input arriving at location x.

Example: Stationary solutions of the cable equation

In order to get an intuitive understanding of the behavior of the cable equation of a passive dendrite we look for stationary solutions of Eq. (3.17), i.e., for solutions with $\partial u(t,x)/\partial t = 0$. In that case, the partial differential equation reduces to an ordinary differential equation in x, namely

$$\frac{\partial^2}{\partial x^2} u(t,x) - u(t,x) = -i_{\text{ext}}(t,x)\,. \tag{3.18}$$

The general solution to the homogenous equation with $i_{\text{ext}}(t,x) \equiv 0$ is

$$u(t,x) = c_1 \sinh(x) + c_2 \cosh(x)\,, \tag{3.19}$$

as can easily be checked by taking the second derivative with respect to x. Here, c_1 and c_2 are constants that are determined by the boundary conditions.

Solutions for non-vanishing input current can be found by standard techniques. For a stationary input current $i_{\text{ext}}(t,x) = \delta(x)$ localized at $x = 0$ and boundary conditions $u(\pm\infty) = 0$ we find

$$u(t,x) = \frac{1}{2}\,\mathrm{e}^{-|x|}; \tag{3.20}$$

see Fig. 3.6. This solution is given in units of the intrinsic length scale $\lambda = (r_{\text{T}}/r_{\text{L}})^{1/2}$. If we re-substitute the physical units, we see that λ is the length over which the stationary membrane potential drops by a factor $1/\mathrm{e}$. In the literature λ is referred to as the electrotonic length scale (Rall, 1989). Typical values for the specific resistance of the intracellular medium and the cell membrane are $100\,\Omega\,\text{cm}$ and $30\text{k}\,\Omega\,\text{cm}^2$, respectively. In a dendrite with radius $\rho = 1\,\mu\text{m}$ this amounts to a longitudinal and a transversal resistance of $r_{\text{L}} = 100\,\Omega\text{cm}/(\pi\rho^2) = 3 \times 10^5\,\Omega\,\mu\text{m}^{-1}$ and $r_{\text{T}} = 30\text{k}\Omega\text{cm}^2/(2\pi\rho) = 5 \times 10^{11}\,\Omega\,\mu\text{m}$. The corresponding electrotonic length scale is $\lambda = 1.2\,\text{mm}$. Note that the electrotonic

https://doi.org/10.1017/CBO9781107447615.004 Published online by Cambridge University Press

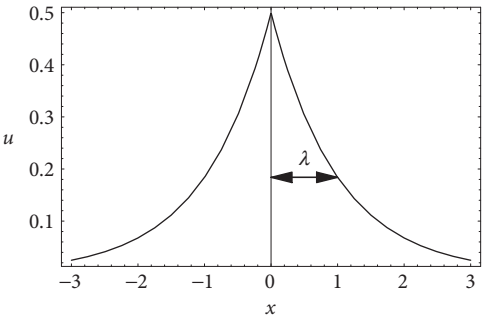

Fig. 3.6 Stationary solution of the cable equation with a constant current of unit strength being injected at $x = 0$, i.e., $i_{\text{ext}}(t,x) = \delta(x)$. The electrotonic length scale λ is the distance over which the membrane potential drops to $1/\text{e}$ of its initial value.

length can be significantly smaller if the transversal conductivity is increased, e.g., due to open ion channels.

For arbitrary stationary input current $i_{\text{ext}}(x)$ the solution of Eq. (3.17) can be found by a superposition of translated fundamental solutions (3.20), namely

$$u(t,x) = \int \mathrm{d}x' \, \frac{1}{2} \, \mathrm{e}^{-|x-x'|} \, i_{\text{ext}}(x') \,. \tag{3.21}$$

This is an example of the Green's function approach applied here to the stationary case. The general time-dependent case will be treated in the next section.

3.2.2 Green's function of the passive cable

In the following we will concentrate on the equation for the voltage and start our analysis by a discussion of the Green's function for a cable extending to infinity in both directions. The Green's function is defined as the solution of a linear equation such as Eq. (3.17) with a Dirac δ-pulse as its input. It can be seen as an elementary solution of the differential equation because – due to linearity – the solution for any given input can be constructed as a superposition of these Green's functions.

Suppose a short current pulse $i_{\text{ext}}(t,x)$ is injected at time $t = 0$ at location $x = 0$. As we will show below, the time course of the voltage at an arbitrary position x is given by

$$u(t,x) = \frac{\Theta(t)}{\sqrt{4\pi t}} \exp\left[-t - \frac{x^2}{4t}\right] \equiv G_\infty(t,x) \,, \tag{3.22}$$

where $G_\infty(t,x)$ is the Green's function. Knowing the Green's function, the general solution for an infinitely long cable is given by

$$u(t,x) = \int_{-\infty}^{t} \mathrm{d}t' \int_{-\infty}^{\infty} \mathrm{d}x' \; G_\infty(t-t', x-x') \, i_{\text{ext}}(t',x') \,. \tag{3.23}$$

The Green's function is therefore a particularly elegant and useful mathematical tool: once you have solved the linear cable equation for a single short current pulse, you can write down the full solution to arbitrary input as an integral over (hypothetical) pulse-inputs at all places and all times.

https://doi.org/10.1017/CBO9781107447615.004 Published online by Cambridge University Press

Checking the Green's property (*)

We can check the validity of Eq. (3.22) by substituting $G_\infty(t,x)$ into Eq. (3.17). After a short calculation we find

$$\left[\frac{\partial}{\partial t} - \frac{\partial^2}{\partial x^2} + 1\right] G_\infty(t,x) = \frac{1}{\sqrt{4\pi t}} \exp\left(-t - \frac{x^2}{4t}\right) \delta(t)\,, \tag{3.24}$$

where we have used $\partial\Theta(t)/\partial t = \delta(t)$. As long as $t \neq 0$ the right-hand side of Eq. (3.24) vanishes, as required by Eq. (3.28). For $t \to 0$ we find

$$\lim_{t\to 0} \frac{1}{\sqrt{4\pi t}} \exp\left(-t - \frac{x^2}{4t}\right) = \delta(x)\,, \tag{3.25}$$

which proves that the right-hand side of Eq. (3.24) is indeed equivalent to the right-hand side of Eq. (3.28).

Having established that

$$\left[\frac{\partial}{\partial t} - \frac{\partial^2}{\partial x^2} + 1\right] G_\infty(t,x) = \delta(x)\,\delta(t)\,, \tag{3.26}$$

we can readily show that Eq. (3.23) is the general solution of the cable equation for arbitrary input currents $i_{\rm ext}(t_0,x_0)$. We substitute Eq. (3.23) into the cable equation, exchange the order of integration and differentiation, and find

$$\begin{aligned}
&\left[\frac{\partial}{\partial t} - \frac{\partial^2}{\partial x^2} + 1\right] u(t,x) \\
&\qquad = \int_{-\infty}^{t} \mathrm{d}t' \int_{-\infty}^{\infty} \mathrm{d}x' \left[\frac{\partial}{\partial t} - \frac{\partial^2}{\partial x^2} + 1\right] G_\infty(t-t',x-x')\, i_{\rm ext}(t',x') \\
&\qquad = \int_{-\infty}^{t} \mathrm{d}t' \int_{-\infty}^{\infty} \mathrm{d}x'\, \delta(x-x')\,\delta(t-t')\, i_{\rm ext}(t',x') = i_{\rm ext}(t,x)\,.
\end{aligned} \tag{3.27}$$

Derivation of the Green's function (*)

Previously, we have just "guessed" the Green's function and then shown that it is indeed a solution of the cable equation. However, it is also possible to derive the Green's function step by step. In order to find the Green's function for the cable equation we thus have to solve Eq. (3.17) with $i_{\rm ext}(t,x)$ replaced by a δ-impulse at $x = 0$ and $t = 0$

$$\frac{\partial}{\partial t} u(t,x) - \frac{\partial^2}{\partial x^2} u(t,x) + u(t,x) = \delta(t)\,\delta(x)\,. \tag{3.28}$$

Fourier transformation with respect to the spatial variable yields

$$\frac{\partial}{\partial t} u(t,k) + k^2\, u(t,k) + u(t,k) = \delta(t)/\sqrt{2\pi}\,. \tag{3.29}$$

This is an ordinary differential equation in t and has a solution of the form

$$u(t,k) = \exp\left[-\left(1+k^2\right) t\right] / \sqrt{2\pi}\,\Theta(t), \tag{3.30}$$

https://doi.org/10.1017/CBO9781107447615.004 Published online by Cambridge University Press

with $\Theta(t)$ denoting the Heaviside function. After an inverse Fourier transform we obtain the desired Green's function $G_\infty(t,x)$,

$$u(t,x) = \frac{\Theta(t)}{\sqrt{4\pi t}} \exp\left[-t - \frac{x^2}{4t}\right] \equiv G_\infty(t,x)\,. \tag{3.31}$$

Example: Finite cable

Real cables do not extend from $-\infty$ to $+\infty$ and we have to take extra care to correctly include boundary conditions at the ends. We consider a finite cable extending from $x=0$ to $x=L$ with sealed ends, i.e., $i(t,x=0)=i(t,x=L)=0$ or, equivalently, $\frac{\partial}{\partial x}u(t,x=0)=\frac{\partial}{\partial x}u(t,x=L)=0$.

The Green's function $G_{0,L}$ for a cable with sealed ends can be constructed from G_∞ by applying a trick from electrostatics called "mirror charges" (Jackson, 1962). Similar techniques can also be applied to treat branching points in a dendritic tree (Abbott, 1991). The cable equation is linear and, therefore, a superposition of two solutions is also a solution. Consider a δ-current pulse at time t_0 and position x_0 somewhere along the cable. The boundary condition $\frac{\partial}{\partial x}u(t,x=0)=0$ can be satisfied if we add a second, virtual current pulse at a position $x=-x_0$ *outside* the interval $[0,L]$. Adding a current pulse outside the interval $[0,L]$ comes for free since the result is still a solution of the cable equation on that interval. Similarly, we can fulfill the boundary condition at $x=L$ by adding a mirror pulse at $x=2L-x_0$. In order to account for both boundary conditions simultaneously, we have to compensate for the mirror pulse at $-x_0$ by adding another mirror pulse at $2L+x_0$ and for the mirror pulse at $x=2L-x_0$ by adding a fourth pulse at $-2L+x_0$ and so forth. Altogether we have

$$G_{0,L}(t_0,x_0;t,x) = \sum_{n=-\infty}^{\infty} G_\infty(t-t_0,x-2nL-x_0) + G_\infty(t-t_0,x-2nL+x_0)\,. \tag{3.32}$$

We emphasize that in the above Green's function we have to specify both (t_0,x_0) and (t,x) because the setup is no longer translation invariant. The general solution on the interval $[0,L]$ is given by

$$u(t,x) = \int_{-\infty}^{t} \mathrm{d}t_0 \int_0^L \mathrm{d}x_0\, G_{0,L}(t_0,x_0;t,x)\, i_{\mathrm{ext}}(t_0,x_0)\,. \tag{3.33}$$

An example for the spatial distribution of the membrane potential along the cable is shown in Fig. 3.7a, where a current pulse has been injected at location $x=1$. In addition to Fig. 3.7a, Fig. 3.7b exhibits the *time course* of the membrane potential measured in various distances from the point of injection. It is clearly visible that the peak of the membrane potential measured at, say, $x=3$ is more delayed than at, say, $x=2$. Also the amplitude of the membrane potential decreases significantly with the distance from the injection point. This is a well-known phenomenon that is also present in neurons. In the absence of active amplification mechanisms, synaptic input at distal dendrites produces

https://doi.org/10.1017/CBO9781107447615.004 Published online by Cambridge University Press

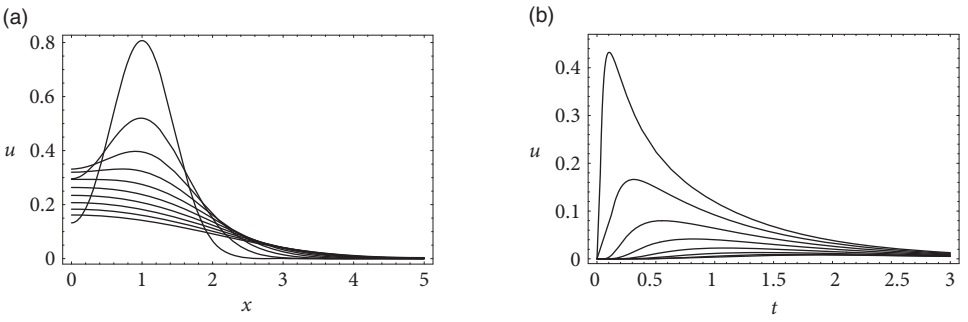

Fig. 3.7 Spatial distribution (a) and temporal evolution (b) of the membrane potential along a dendrite ($L = 5$) with sealed ends $\left(\frac{\partial}{\partial x} u \Big|_{x \in \{0,L\}} = 0 \right)$ after injection of a unit current pulse at $x = 1$ and $t = 0$. The various traces in (a) show snapshots for time $t = 0.1, 0.2, \ldots, 1.0$, respectively (top to bottom). The traces in (b) give the membrane potential as a function of time for different locations $x = 1.5, 2.0, 2.5, \ldots, 5.0$ (top to bottom) along the cable.

broader and weaker response at the soma as compared to synaptic input at proximal dendrites.

3.2.3 Nonlinear extensions to the cable equation

In the context of a realistic modeling of "biological" neurons, two nonlinear extensions of the cable equation have to be discussed. The obvious one is the inclusion of nonlinear elements in the circuit diagram of Fig. 3.5 that account for specialized ion channels. As we have seen in the Hodgkin–Huxley model, ion channels can exhibit a complex dynamics that is in itself governed by a system of (ordinary) differential equations. The current through one of these channels is thus not simply a (nonlinear) function of the actual value of the membrane potential but may also depend on the time course of the membrane potential in the past. Using the symbolic notation $i_{\text{ion}}[u](t,x)$ for this functional dependence, the extended cable equation takes the form

$$\frac{\partial}{\partial t} u(t,x) = \frac{\partial^2}{\partial x^2} u(t,x) - u(t,x) - i_{\text{ion}}[u](t,x) + i_{\text{ext}}(t,x) \,. \tag{3.34}$$

A more subtle complication arises from the fact that a synapse cannot be treated as an ideal current source. The effect of an incoming action potential is the opening of ion channels. The resulting current is proportional to the difference of the membrane potential and the corresponding ionic reversal potential. Hence, a time-dependent conductivity as in Eq. (3.1) provides a more realistic description of synaptic input than an ideal current source with a fixed time course.

If we replace in Eq. (3.17) the external input current $i_{\text{ext}}(t,x)$ by an appropriate synaptic input current $-i_{\text{syn}}(t,x) = -g_{\text{syn}}(t,x)[u(t,x) - E_{\text{syn}}]$ with g_{syn} being the synaptic

https://doi.org/10.1017/CBO9781107447615.004 Published online by Cambridge University Press

conductivity and E_{syn} the corresponding reversal potential, we obtain[2]

$$\frac{\partial}{\partial t}u(t,x) = \frac{\partial^2}{\partial x^2}u(t,x) - u(t,x) - g_{\text{syn}}(t,x)[u(t,x) - E_{\text{syn}}]\,. \tag{3.35}$$

This is still a linear differential equation but its coefficients are now time-dependent. If the time course of the synaptic conductivity can be written as a solution of a differential equation, then the cable equation can be reformulated so that synaptic input reappears as an inhomogeneity to an autonomous equation. For example, if the synaptic conductivity is simply given by an exponential decay with time constant τ_{syn} we have

$$\frac{\partial}{\partial t}u(t,x) - \frac{\partial^2}{\partial x^2}u(t,x) + u(t,x) + g_{\text{syn}}(t,x)[u(t,x) - E_{\text{syn}}] = 0\,, \tag{3.36a}$$

$$\frac{\partial}{\partial t}g_{\text{syn}}(t,x) - \tau_{\text{syn}}^{-1}g_{\text{syn}}(t,x) = S(t,x)\,. \tag{3.36b}$$

Here, $S(t,x)$ is a sum of Dirac δ-functions which describe the presynaptic spike train that arrives at a synapse located at position x. Note that this equation is *non*linear because it contains a product of g_{syn} and u which are both unknown functions of the differential equation. Consequently, the formalism based on Green's functions cannot be applied. We have reached the limit of what we can do with analytical analysis alone. To study the effect of ion channels distributed on the dendrites numerical approaches in compartmental models become invaluable (Section 3.4).

3.3 Spatial structure: axons

Any given neuron has a single axon that leaves the soma to make synaptic contacts. Like dendrites, axons have a range of different morphologies. Some axons project mainly to neurons close by. This is the case for neurons in the layer 2–3 of cortex; their axons branch out in all directions from the soma forming a star-shaped axonal arbor called a "daisy." Other neurons such as pyramidal neurons situated deeper in the cortex have axons that plunge in the white matter and may cross the whole brain to reach another brain area. There are even longer axons that leave the central nervous system and travel down the spinal cord to reach muscles at the tip of the foot.

In terms of propagation dynamics, we distinguish two types of axons: the myelinated and the unmyelinated axons. We will see that myelin is useful to increase propagation speed in far-reaching projections. This is the case for cortical projections passing through the white matter, or for axons crossing the spinal cord. Short projections on the other hand use axons devoid of myelin.

3.3.1 Unmyelinated axons

Mathematical description of the membrane potential in the axon is identical to that of dendrites with active ion channels. Unmyelinated axons contain sodium and potassium

[2] We want outward currents to be positive, hence the change in the sign of i_{ext} and i_{syn}.

https://doi.org/10.1017/CBO9781107447615.004 Published online by Cambridge University Press

channels uniformly distributed over their entire length. The classical example is the squid giant axon investigated by Hodgkin and Huxley. The Hodgkin–Huxley model described in Chapter 2 was developed for a small axon segment. The general equation for ion channels imbedded on a passive membrane is

$$c\, r_{\mathrm{L}} \frac{\partial}{\partial t} u(t,x) = \frac{\partial^2}{\partial x^2} u(t,x) - r_{\mathrm{L}}(u(t,x) - E_l) - r_{\mathrm{L}} i_{\mathrm{ion}}[u](t,x) \tag{3.37}$$

where we have reverted to a variable u in units of mV from the equation of active dendrites seen in Section 3.2.3. For the giant squid axon, the ionic current are described by the Hodgkin–Huxley model

$$i_{\mathrm{ion}}[u](t,x) = g_{\mathrm{Na}}\, m^3(t,x) h(t,x)\,(u(t,x) - E_{\mathrm{Na}}) + g_{\mathrm{K}}\, n^4(t,x)\,(u(t,x) - E_{\mathrm{K}}). \tag{3.38}$$

In other systems, the axon may be covered with other types of sodium or potassium ion channels.

When an action potential is fired in the axon initial segment, the elevated membrane potential will depolarize the adjacent axonal segments. Sodium channels farther down the axon, which were previously closed, will start to open, thereby depolarizing the membrane further. The action potential propagates by activating sodium channels along the cable rather than by spreading the charges as in a passive dendrite. The properties of the ion channels strongly influence conduction velocity. In the unmyelinated axons of the hippocampus, the conduction velocity of the axons is 0.25 m/s.

The dynamics described by Eqs. (3.37)–(3.38) reproduces many properties of real axons. In particular, two spikes traveling in opposite direction will collide and annihilate each other. This is unlike waves propagating on water. Another property is reflection at branch points. When the impedance mismatch at the point where a single axon splits into two is significant, the action potential can reflect and start traveling in the direction it came from.

The solution of Eq. (3.37) with sodium and postassium ion channels as in Eq. (3.38) cannot be written in a closed form. Properties of axonal propagation are either studied numerically (see Section 3.4) or with reduced models of ion channels.

Example: Speed of propagation with simplified action potential dynamics

For the sake of studying propagation properties, we can replace the active properties of a small axonal segment by a bistable switch (FitzHugh, 1961; Nagumo *et al.*, 1962) . We can write the time- and space-dependent membrane potential as

$$c\, r_{\mathrm{L}} \frac{\partial}{\partial t} u(t,x) = \frac{\partial^2}{\partial x^2} u(t,x) - \frac{r_{\mathrm{L}} g}{1-a} u(t,x)(u(t,x)-1)(u(t,x)-a)\,, \tag{3.39}$$

where $a < 1/2$ and g are parameters. The membrane potential is scaled such that it rests at zero but may be activated to $u = 1$. The reduced model can switch between $u = 0$ and $u = 1$ if it is pushed above $u = a$, but does not reproduce the full upswing followed by downswing of action potentials.

https://doi.org/10.1017/CBO9781107447615.004 Published online by Cambridge University Press

It turns out that Eq. (3.39) can also be interpreted as a model of flame front propagation. The solution of this equation follows (Zeldovich and Frank-Kamenetskii, 1938)

$$u(x,t) = \frac{1}{1+\exp\left(\frac{x-\mathsf{v}t}{\sqrt{2}\lambda^*}\right)} \tag{3.40}$$

with traveling speed

$$\mathsf{v} = \frac{c(1-2a)}{\sqrt{2(1-a)r_{\mathrm{L}}/g}}. \tag{3.41}$$

The propagation velocity depends on the capacitance per unit length c, the longitudinal resistance per unit length r_{L}, and the excitability parameters g and a.

How does the conduction velocity scale with axon size? Since r_{L}, c and g themselves depend on the diameter of the axon, we expect the velocity to reflect that relationship. The parameters c and g scale with the circumference of the cellular membrane and therefore scale linearly with the radius ρ. The cytoplasmic resistance per unit length, however, scales with the cross-sectional area, $r_{\mathrm{L}} \propto \rho^2$. With these relations in mind, Eq. (3.41) shows that the conduction velocity is proportional to the square root of the diameter $\mathsf{v} \propto \sqrt{\rho}$. Therefore, increasing the diameter improves propagation velocity. This is thought to be the reason why the unmyelinated axons that Hodgkin and Huxley studied were so large (up to $\rho = 500\,\mu\mathrm{m}$).

3.3.2 Myelinated axons

Myelinated axons have sodium and potassium channels only in restricted segments called *nodes of Ranvier*. These nodes form only 0.2% of the axonal length, the rest is considered a passive membrane that is wrapped into a myelin sheath. Myelin mainly decreases the membrane capacitance C and increase the resistance R_T by a factor of up to 300 (Debanne *et al.*, 2011). Ions are trapped by myelin since it prevents them from either flowing outside the axon or accumulating on the membrane. Instead, ions flow in and out of the nodes such that an ion leaving a node of Ranvier forces another to enter the following node. Assuming that the nodes are equally separated by a myelinated segment of length L, we can model the evolution of the membrane potential at each node u_n. The dynamics of idealized myelinated axons follow Kirchoff's equation with a resistance $R_{\mathrm{L}} = L r_L$ replacing the myelinated segment

$$C\frac{\mathrm{d}u_n}{\mathrm{d}t} = \frac{1}{L r_{\mathrm{L}}}(u_{n+1}(t) - 2u_n(t) + u_{n-1}(t)) - \sum_{\mathrm{ion}} I_{\mathrm{ion},n}(t) \tag{3.42}$$

where C is the total capacitance of the node. This equation was encountered in the derivation of the cable equation (Section 3.2.1). The conduction velocity is greatly increased by myelin such that some nerves reach 70–80 m/s (Debanne *et al.*, 2011).

https://doi.org/10.1017/CBO9781107447615.004 Published online by Cambridge University Press

Example: Propagation speed with simplified action potential dynamics

Using the simplification of the ion channel dynamics in Eq. (3.39) for each node

$$C\frac{\mathrm{d}u_n}{\mathrm{d}t} = \frac{1}{Lr_\mathrm{L}}(u_{n+1}(t) - 2u_n(t) + u_{n-1}(t)) - \frac{g}{1-a}u_n(t)(u_n(t)-1)(u_n(t)-a) \quad (3.43)$$

where g and $a < 1/2$ are parameters regulating the excitability of the node. Unlike Eq. (3.39), the parameter g has units of conductance per node since the nodes of Ranvier are discrete segments. An activated node may fail to excite the adjacent nodes if the membrane potential does not reach $u = a$. In this model, the internodal distance must satisfy (Erneux and Nicolis, 1993)

$$L < L^* = \frac{1-a}{4a^2 r_\mathrm{L} g} \quad (3.44)$$

for propagation to be sustained. When the internodal distance L is smaller than L^*, propagation will fail. When the internodal distance is larger, propagation will succeed.

The propagation velocity for small $L^* - L$ follows (Binczak *et al*., 2001)

$$\mathsf{v} \approx \frac{\pi g a}{(1-a)C}\sqrt{L(L^*-L)} \quad (3.45)$$

which is maximum at $L = L^*/2$. Since, in most myelinated axons, internodal distance scales linearly with their radius (Waxman, 1980), the velocity of myelinated axons also scales linearly with radius, $\mathsf{v} \propto L \propto \rho$.

3.4 Compartmental models

We have seen that analytical solutions can be given for the voltage along a passive cable with uniform geometrical and electrical properties. If we want to apply the above results in order to describe the membrane potential along the dendritic tree of a neuron we face several problems. Even if we neglect "active" conductances formed by nonlinear ion channels, a dendritic tree is at most *locally* equivalent to a uniform cable. Numerous bifurcations and variations in diameter and electrical properties along the dendrite render it difficult to find a solution for the membrane potential analytically (Abbott *et al*., 1991).

Numerical treatment of partial differential equations such as the cable equation requires a discretization of the spatial variable. Hence, all derivatives with respect to spatial variables are approximated by the corresponding quotient of differences. Essentially we are led back to the discretized model of Fig. 3.5 that has been used as the starting point for the derivation of the cable equation. After the discretization we have a large system of ordinary differential equations for the membrane potential at the chosen discretization points as a function of time. This system of ordinary differential equations can be treated by standard numerical methods.

https://doi.org/10.1017/CBO9781107447615.004 Published online by Cambridge University Press

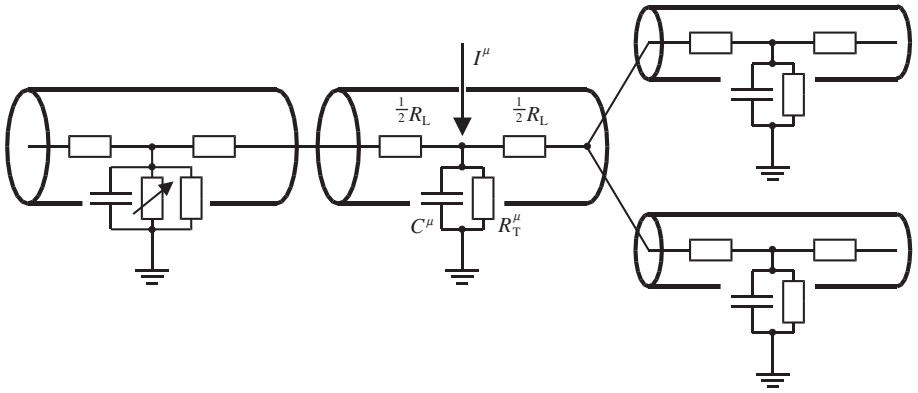

Fig. 3.8 Multi-compartment neuron model. Dendritic compartments with membrane capacitance C^μ and transversal resistance R_T^μ are coupled by a longitudinal resistance $r^{\mu\nu} = (R_L^\mu + R_L^\nu)/2$. External input to compartment μ is denoted by I^μ. Some or all compartments may also contain nonlinear ion channels (variable resistor in leftmost compartment).

In order to solve for the membrane potential of a complex dendritic tree numerically, compartmental models are used that are the result of the above mentioned discretization. The dendritic tree is divided into small cylindric compartments with an approximatively uniform membrane potential. Each compartment is characterized by its capacity and transversal conductivity. Adjacent compartments are coupled by the longitudinal resistance determined by their geometrical properties (see Fig. 3.8).

Once numerical methods are used to solve for the membrane potential along the dendritic tree, some or all compartments can be equipped with nonlinear ion channels as well. In this way, effects of nonlinear integration of synaptic input can be studied. Apart from practical problems that arise from a growing complexity of the underlying differential equations, conceptual problems are related to a drastically increasing number of free parameters. To avoid these problems, all nonlinear ion channels responsible for generating spikes are usually lumped together at the soma and the dendritic tree is treated as a passive cable. For a review of the compartmental approach we refer the reader to Bower and Beeman (1995). In the following we illustrate the compartmental approach by a model of a pyramidal cell.

Example: A multi-compartment model of a deep-layer pyramidal cell

Software tools such as NEURON (Carnevale and Hines, 2006) or GENESIS (Bower and Beeman, 1995) enable researchers to construct detailed compartmental models of any type of neuron. The morphology of such a detailed model is constrained by the anatomical reconstruction of the corresponding "real" neuron. This is possible if length,

https://doi.org/10.1017/CBO9781107447615.004 Published online by Cambridge University Press

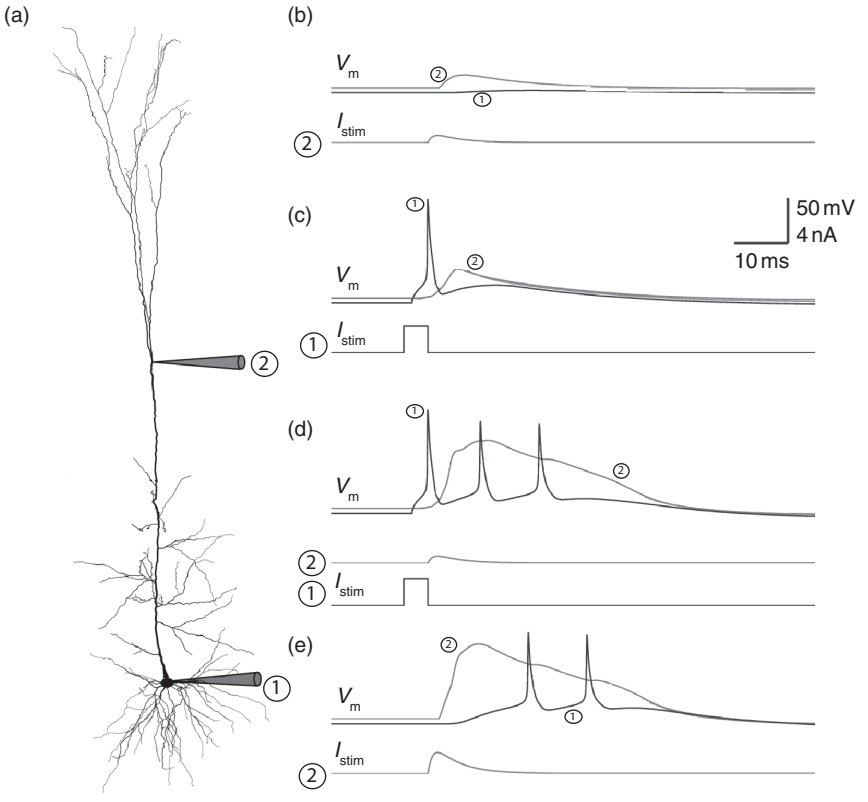

Fig. 3.9 Bursting in a computational model of a deep layer cortical neuron. (a) Reconstruction of the complete morphology indicating the location of injection and measurement sites marked "1" at the soma, and "2" at the dendrite. (b) A current is injected into the dendrite (lower trace, marked "2") mimicking an excitatatory postsynaptic current (EPSC). The model responds to the current injection in the dendrite with a voltage deflection at the dendrite (upper trace marked "2") but hardly any deflection at the soma ("1"). (c). A current pulse in the soma (lower trace, marked "1") causes an action potential at the soma (voltage trace marked "1") that back-propagates as a broader voltage pulse ("2") into the dendrite. (d) Coincidence of somatic current pulse and dendritic EPSC activates calcium currents in the dendrites and causes a burst of spikes in the soma. (e) A single, but large EPSC-shaped dendritic current can also activate calcium currents and leads to a delayed burst of spikes in the soma. Image modified from Hay *et al.* (2011).

size and orientation of each dendritic segment are measured under a microscope, after the neuron has been filled with a suitable dye. Before the anatomical reconstruction, the electrophysiological properties of the neuron can be characterized by stimulating the neuron with a time-dependent electric current. The presence of specific ion channel types can be inferred, with genetic methods, from the composition of the intracellular liquid, extracted from the neuron (Toledo-Rodriguez *et al.*, 2004). The distribution of ion

https://doi.org/10.1017/CBO9781107447615.004 Published online by Cambridge University Press

channels across the dendrite is probably the least constrained parameter. It is sometimes inferred from another set of experiments on neurons belonging to the same class. All the experimental knowledge about the neuron is then condensed in a computational neuron model. A good example is the model of a deep-layer cortical neuron with active dendrites as modeled by Hay *et al.* (2011).

The complete morphology is divided into 200 compartments, none exceeding 20 μm in length. Each compartment has its specific dynamics defined by intracellular ionic concentration, transversal ion flux through modeled ion channels, and longitudinal current flux to connected compartments. The membrane capacitance is set to 1 $\mu F/cm^2$ for the soma and axon and to 2 $\mu F/cm^2$ in the dendrites to compensate for the presence of dendritic spines. A cocktail of ionic currents is distributed across the different compartments. These are:

- the fast inactivating sodium current I_{Na} (Section 2.2.1),
- the persistent sodium current I_{NaP} (Section 2.3.3),
- the non-specific cation current I_h (Section 2.3.4),
- the muscarinic potassium current I_M (Section 2.3.3),
- the small conductance calcium-activated potassium current $I_{K[Ca]}$ (Section 2.3.4),
- the fast non-inactivating potassium current $I_{Kv3.1}$ (Rettig *et al.*, 1992) which is very similar to the model of potassium current of the Hodgkin–Huxley model in Table 2.1,
- the high-voltage activated calcium current I_{HVA} (mentioned in Section 2.3.3),
- the low-voltage activated calcium current I_L(Avery and Johnston, 1996; Randall and Tsien, 1997) (similar to the HVA channel but different parameters),
- and a calcium pump (Section 2.3.3).

In addition, the model contains a slow and a fast inactivating potassium current I_{Kp}, I_{Kt}, respectively (Korngreen and Sakmann, 2000).

In the dendrites all these currents are modeled as uniformly distributed except I_h, I_{HVA} and I_L. The first one of these, I_h, is exponentially distributed along the main dendrite that ascends from the deep layers with low I_h concentration to the top layers with large I_h concentration (Kole *et al.*, 2006). The two calcium channels were distributed with a uniform distribution in all dendrites except for a single hotspot with a concentration 100 and 10 times higher for I_L and I_{HVA}, respectively. Finally, the strength of each ionic current was scaled by choosing the maximal conductance g_{ion} that best fit experimental data.

This detailed compartmental model can reproduce quantitatively some features of the deep-layer pyramidal neurons (Fig. 3.9). For example, a small dendritic current injection results in a transient increase of the dendritic voltage, but only a small effect in the soma (Fig. 3.9b). A sufficiently large current pulse in the soma initiates not only a spike at the soma but also a back-propagating action potential traveling into the dendrites (Fig. 3.9c). Note that it is the presence of sodium and potassium currents throughout the dendrites that support the back-propagation. In order to activate the dendritic calcium channels at the hotspot, either a large dendritic injection or a coincidence between the

back-propagating action potential and a small dendritic injection is required (Fig. 3.9d, e). The activation of calcium channels in the hotspot introduces a large and long (around 40 ms) depolarizing current that propagates forward to the soma where it eventually causes a burst of action potentials.

3.5 Summary

"Real" neurons are complex biophysical and biochemical entities. Before designing a model it is therefore necessary to develop an intuition for what is important and what can be safely neglected. Synapses are usually modeled as specific ion channels that open for a certain time after presynaptic spike arrival. The geometry of the neuron can play an important role in the integration of incoming signals because the effect of synaptic input on the somatic membrane potential depends on the location of the synapses on the dendritic tree. Though some analytic results can be obtained for *passive* dendrites, it is usually necessary to resort to numerical methods and multi-compartment models in order to account for the complex geometry and presence of active ion channels on neuronal dendrites.

Literature

The book *Dendrites* (Stuart *et al*., 2007) offers a comprehensive review of the role and importance of dendrites from multiple points of view. An extensive description of cable theory as applied to neuronal dendrites can be found in the collected works of Wilfrid Rall (Segev *et al*., 1994). NEURON (Carnevale and Hines, 2006) and GENESIS (Bower and Beeman, 1995) are important tools to numerically solve the system of differential equations of compartmental neuron models. There are useful repositories of neuronal morphologies (see http://NeuroMorpho.Org for instance) and of published models on ModelDB (http://senselab.med.yale.edu/modeldb). The deep-layer cortical neuron discussed in this chapter is described in Hay *et al*. (2011). Potential computational consequences of nonlinear dendrites are described in Mel (1994).

Exercises

1. **Biophysical synapse model and its relation to other models**
   (a) Consider Eq. (3.4) and discuss its relation to Eq. (3.2). Hint: (i) Assume that the time course $\gamma(t)$ *can be described by a short pulse (duration of* 1 ms*) and that the unbinding is on a time scale* $\beta^{-1} > 10\,\text{ms}$*. (ii) Assume that the interval between two presynaptic spike arrivals is much larger than* β^{-1}*.*
   (b) Discuss the relation of the depressive synapse model in Eq. (3.8) with the biophysically model in Eq. (3.4). Hint: (i) Assume that the interval between two presynaptic spikes is of the same order β^{-1}*. (ii) In Eq. (3.8) consider a variable* $x = P_{\text{rel}}/P_0$*.*

https://doi.org/10.1017/CBO9781107447615.004 Published online by Cambridge University Press

2. **Transmitter-gated ion channel**
   For each of the following statements state whether it is correct or wrong:
   (a) AMPA channels are activated by glutamate.
   (b) AMPA channels are activated by AMPA.
   (c) If the AMPA channel is open, AMPA can pass through the channel.
   (d) If the AMPA channel is open, glutamate can pass through the channel.
   (e) If the AMPA channel is open, potassium can pass through the channel.
3. **Cable equation**
   (a) Show that the passive cable equation for the current is

$$\frac{\partial}{\partial t} i(t,x) = \frac{\partial^2}{\partial x^2} i(t,x) - i(t,x) + \frac{\partial}{\partial x} i_{\text{ext}}(t,x). \tag{3.46}$$

   (b) Set the external current to zero and find the mapping to the heat equation

$$\frac{\partial}{\partial t} y(t,x) = \frac{\partial^2}{\partial x^2} y(t,x). \tag{3.47}$$

   Hint: Try $y(t,x) = f(t)\, i(t,x)$ with some function f.
   (c) Find the solution to the current equation in (a) for the infinite cable receiving a short current pulse at time $t = 0$ and show that the corresponding equation for y satisfies the heat equation in (b).
4. **Non-leaky cable**
   (a) Redo the derivation of the cable equation for the case of an infinite one-dimensional passive dendrite without transversal leak and show that the solution to the equation is of the form

$$u(x,t) = \int_{-\infty}^{t} \mathrm{d}t' \int_{-\infty}^{\infty} \mathrm{d}x'\, G_d(t-t', x-x')\, i_{\text{ext}}(t',x') \tag{3.48}$$

   where G_d is a Gaussian of the form

$$G_d(x,t) = \frac{1}{\sqrt{2\pi\sigma(t)}} \exp - \frac{x^2}{2\sigma^2(t)}. \tag{3.49}$$

   Determine $\sigma(t)$ and discuss the result.
   (b) Use the method of mirror charges to discuss how the solution changes if the cable is semi-infinite and extends from zero to infinity.
   (c) Take the integral over space of the elementary solution of the non-leaky cable equation and show that the value of the integral does not change over time. Give an interpretation of this result.
   (d) Take the integral over space of the elementary solution of the normal leaky cable equation of a passive dendrite and derive an expression for its temporal evolution. Give an interpretation of your result.
5. **Conduction velocity in unmyelinated axons**
   (a) Using the simplified ion channel dynamics of Eq. (3.39), transform x and t to dimensionless variables using effective time and electrotonic constants.
   (b) A traveling pulse solution will have the form $u(x,t) = \tilde{u}(x - \mathsf{v}t)$ where v is the conduction velocity. Find the ordinary differential equation that rules $\tilde{u}$.
   (c) Show that $\tilde{u}(y) = \frac{1}{1+\exp(y)}$ with traveling speed $\mathsf{v} = \frac{1-2a}{\sqrt{2}}$ is a solution.

https://doi.org/10.1017/CBO9781107447615.004 Published online by Cambridge University Press